

Emergent anisotropy and textures in two dimensional magnetic arrays

Nanny Strandqvist¹, Björn Erik Skovdal¹, Merlin Pohlitz¹, Henry Stopfel¹, Lisanne van Dijk,²
Vassilios Kapaklis¹, and Björgvin Hjörvarsson¹

¹Department of Physics and Astronomy, Uppsala University, Box 516, SE-75120 Uppsala, Sweden

²Department of Applied Physics, Eindhoven University of Technology, P.O. Box 513, 5600 MB Eindhoven, The Netherlands



(Received 10 May 2022; accepted 18 October 2022; published 31 October 2022)

We demonstrate the presence of an emergent magnetic anisotropy in square lattices of circular mesospins. An external field is used to saturate the magnetization along the [10] and [11] directions before quantifying the magnetic textures at remanence. A clear directional dependence was obtained. The concomitant changes in the interactions are argued to cause the observed anisotropy and, thereby, the directional dependence in the transition temperature of the mesospins.

DOI: [10.1103/PhysRevMaterials.6.105201](https://doi.org/10.1103/PhysRevMaterials.6.105201)

I. INTRODUCTION

Magnetic metamaterials can be used for investigations of phase transitions with a control of system parameters only surpassed by numerical methods [1–8]. In these studies, the magnetic islands—*mesospins*—have often been treated as indivisible building blocks without inner structure with a classical order-disorder transition of the mesoscopic elements. It is only recently their inner degrees of freedom have been included in the description [9–12]. For disk-shaped mesospins, a collection of works addressed dynamics involving bistability of magnetization textures within, depending on geometry and temperature [13,14]. It was further shown that the size and shape of the mesospins determines also to which extent static internal S- or C-like-shaped magnetic textures and collinear or vortex states, prevail [15–18]. A more detailed understanding of the role of thermal excitations in the magnetic texture was only recently developed [9,11,12]. In the light of this, systems allowing for the study of the effect of internal mesospin degrees of freedom on the collective order and thermal dynamics, have been shown to exhibit exotic order-disorder transitions [9,19]. In all of these cases, circular magnetic islands effectively act as XY spins with variable spin lengths.

The emergence of an anisotropy in magnetic metamaterials has previously been demonstrated and attributed to geometrical parameters: mesospin shape and lattice symmetry [20–22]. Here, we show that the internal magnetic textures of disk-shaped mesospins, along with their local magnetization configurations also play an essential role. The directional dependence is shown to originate from an interplay between

the extension of the elements and the symmetry of the lattice, giving rise to a self-induced-anisotropy for the interelement interactions. Thus, the internal degrees of freedom lead to an emergent magnetic anisotropy on the mesoscale, which is neither present in the parent material nor in the individual mesospins. Furthermore, we show that the strength of the anisotropy can be altered by the size of the mesospin, effectively allowing for the choice of fourfold or eightfold rotational degeneracy of metastable states with collinear magnetization components.

II. MATERIALS AND METHODS

The samples were produced by postpatterning a polycrystalline three-layer thin film using electron-beam lithography. The thin films consisted of Pd (40 nm)—Fe₁₃Pd₈₇ (10 nm)—Pd (2 nm) and were deposited by DC magnetron sputtering on a fused silica substrate in an ultrahigh-vacuum (base pressure below 2×10^{-7} Pa). A detailed description of the complete process can be found in Skovdal et al. [9]. The periodic square arrays of circular mesospins were fabricated with a fixed edge-to-edge distance of 20 nm and diameters of $D = 250, 350, \text{ and } 450$ nm. The temperature dependence of the metamaterial magnetization was determined using standard magneto-optical Kerr effect in a longitudinal mode [9]. The incident wavelength of the p -polarized incident laser was set to 659 nm with a spot size of 1 mm^2 , giving the response of approximately $5\text{--}14 \times 10^6$ mesospins. An external field with an amplitude of 40 mT was applied along the [10] and [11] directions with a sweep rate of 0.11 Hz.

The interplay of interelement coupling and the mesospin magnetic texture was explored by performing micromagnetic simulations, using MuMax³ [23]. Disks, mimicking the actual mesospins, were placed on a 5×5 square lattice with periodic boundary conditions in lateral directions. A saturation magnetization of $M_{\text{sat}} = 3.5 \times 10^5 \text{ A/M}$, and exchange stiffness of $A_{\text{ex}} = 3.36 \times 10^{-12} \text{ J/m}$, were chosen based on previous works [14,24] using the same alloy. The in-plane cell size was defined as $0.5l_{\text{ex}}$, where the exchange length l_{ex} is a

Published by the American Physical Society under the terms of the Creative Commons Attribution 4.0 International license. Further distribution of this work must maintain attribution to the author(s) and the published article's title, journal citation, and DOI. Funded by Bibsam.

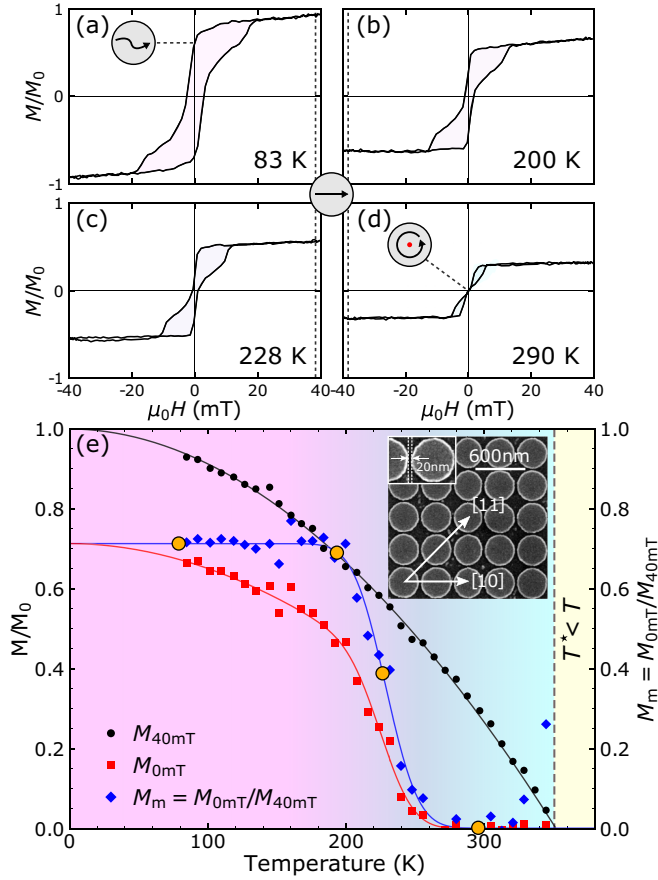


FIG. 1. Top: Magnetization loops at (a) 83, (b) 200, (c) 228, and (d) 290 K for mesospins with diameters of 350 nm, and magnetic field applied along the [10] direction. The curves have been normalized to the net magnetization at $T = 0$, obtained by fitting the magnetization at 40 mT. Illustrations represent possible internal magnetization textures at 40 and 0 mT, respectively. Bottom: Temperature dependence of magnetization $M_{40\text{mT}}$ and $M_{0\text{mT}}$ (left axis) and the ratio $M_m = M_{0\text{mT}}/M_{40\text{mT}}$ (right axis). The yellow dots mark the temperature at which the hysteresis curves were measured. The inset shows a scanning electron microscopy image for a representative structure with disks of a diameter $D = 350$ nm and an edge-to-edge gap of 20 nm. The arrows indicate the principal lattice directions [10] and [11].

material parameter defined by M_{sat} and A_{ex} [25]. The average magnetization $|\langle \mathbf{m} \rangle|$ of the magnetic states in Table I was obtained by saturating disks placed on a 5×5 grid, followed by relaxing the systems to its minimum free energy. Thereafter, each mesospin was extracted, and the net moment along one axis was used as a base for calculating $|\langle \mathbf{m} \rangle|$ and is, therefore, an average of several disks.

III. RESULTS AND DISCUSSION

A. Thermally induced transition

Representative hysteresis loops measured along the [10] direction are shown in the top panel of Figs. 1(a)–1(d) for disk-shaped elements with diameters of 350 nm. At 83 K, a state with a net normalized magnetization of 0.93(2) is obtained when applying a field of 20 mT. When reducing the field, the magnetization decreases, and at zero a remanence

of 0.65(2) is obtained. Profound changes in the magnetization are observed when the temperature is increased. For example, at 290 K, the hysteresis loop has changed form, and a saturation with a net magnetization of 0.32(2) is obtained already at 5 mT whereas zero magnetization is observed at remanence. Hence, the hysteresis loops obtained at elevated temperatures are representative of vortex states [26], whereas the hysteresis loops obtained at low temperatures have clear ferromagnetic components at remanence [9].

The hysteresis loops described above show a clear signature of magnetic textures, which can be removed by sufficiently small fields (< 20 mT). Since weak fields marginally affect the thermally induced reduction of the magnetization, the magnetization (at modest fields) can be viewed as representing the intrinsic magnetization of the material ($M_{40\text{mT}}$) shown in the bottom panel of Fig. 1(e). A modified Bloch law is used to describe the temperature dependence,

$$M_{40\text{mT}}(T) = M_{40\text{mT}}(T = 0)[1 - (T/T^*)^\alpha],$$

where $\alpha = 1.94(3)$ and $T^* = 352(1)$ K, represented by a black solid line in the bottom panel of Fig. 1.

The temperature dependence of the remanent magnetization ($M_{0\text{mT}}$) is symbolized by red squares in Fig. 1(e). The remanence vanishes at 270 K, which is well below the ordering temperature of the material. By dividing the remanent magnetization with the inferred intrinsic magnetization of the material, we can extract the contribution from the magnetic texture to the changes in magnetization ($M_m = M_{0\text{mT}}/M_{40\text{mT}}$) [1,9]. Thus, the reduction of the relative magnetization arising from the presence of inner magnetic textures can be written as $M_T = 1 - M_m$. In the bottom panel of Fig. 1, a plateau with $M_m = 0.71(2)$ is observed at temperatures below 195 K. Consequently, almost 30% of the moment [$M_T = 0.29(2)$] is not contributing to the obtained magnetization. M_m vanishes in a relatively narrow temperature range, and at 270 K, the transition to vortex states is completed. Above this temperature, all the moment is involved in vortex magnetic textures giving rise to a zero collinear magnetization component.

B. Size dependence

Figure 2 illustrates the experimentally determined temperature dependence of M_m for mesospin diameters $D = [250, 350, 450]$ nm with the external field applied along the [10] direction. All samples display an error function like transition. The plateau value of M_m (at $T = 0$) increases with mesospin size and ranges from 0.68(1) to 0.75. Here we note that the smaller the diameter is, the lower the temperature is for the onset of the transition. No clear trends are observed with respect to the temperature when the transition is completed.

To rationalize the size dependence, we need to get a handle on different contributions to the mesospin energy landscape, including the interplay of mesospin interactions and their inner magnetic texture. Therefore, we performed micromagnetic calculations using MuMax³ [23]. The total magnetic energy of the arrays can be defined as: $E_{\text{tot}} = E_t + E_s + E_j$, where E_t is the energy cost of magnetic texture, E_s is the magnetostatic energy arising from the stray field, and E_j is

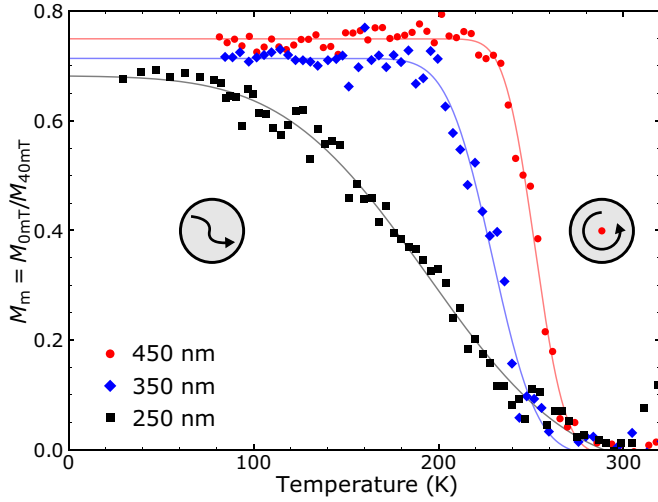


FIG. 2. Temperature dependence of experimentally determined $M_m = M_{0\text{mT}}/M_{40\text{mT}}$ along the [10] direction for mesospins with $D = 250, 350$, and 450 nm. Error functions (solid lines) were chosen in order to determine the transition temperatures. Illustrations exemplify the possible internal texture of a mesospin.

the energy associated with magnetostatic coupling between the mesospins. E_{tot} has been calculated as the vortex cores have been moved along paths, resembling one of many possible trajectories arising from the application of an external magnetic field.

In the vortex state, the energy is only dependent on the cost of texture since $E_s \approx E_j \approx 0$. The results reveal a size dependence where the cost of the vortex state (E_v) decreases with increasing size. Moreover, moving the vortex core from the center of a mesospin results in a collinear magnetic component with a corresponding stray field, leading to coupling between the mesospins. Consequently, the energy increases, reaching a maximum at $2r/D \approx 0.9$. Continuing to move the vortex cores results in an energy decrease. When the cores have been annihilated (at the rim, $2r/D = 1$), all mesospins possess a magnetic texture resembling a C state. The degree of texture continues to change with the displacement of the virtual vortex core outside the rim, and the energy is observed to decrease until reaching the collinear state. The activation energies (energy barriers) separating the collinear and vortex states are asymmetric as seen in the figure.

The inset in Fig. 3 shows the energy difference of the vortex and collinear state ($E_v - E_c$) as a function of $1/D$. The linear fit reveals that for $D \lesssim 190$ nm, the collinear state is the ground state, whereas a vortex state is favored when the diameter is larger. Thus, the vortex is the ground state for all the samples that are experimentally investigated here. Consequently, the elements can be viewed as being “dressed” by the external field, inducing a change in energy and giving rise to a ferromagnetic signal in the measurements. Before addressing the importance of these two contributions, we investigate what happens when the direction of the net magnetization of the elements changes.

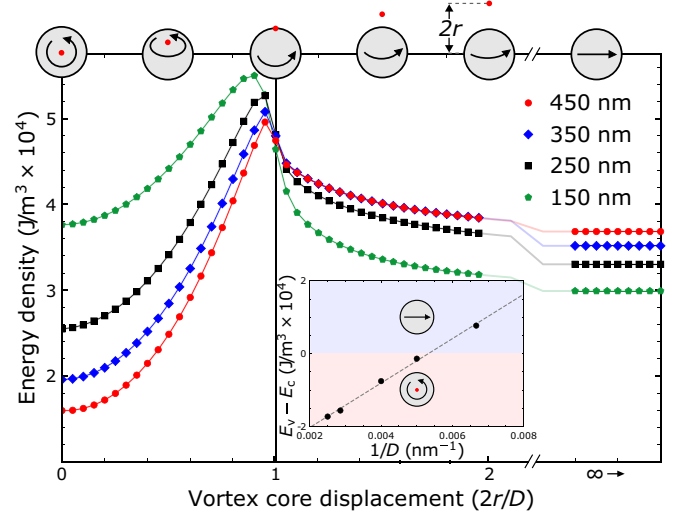


FIG. 3. Energy densities from micromagnetic simulations for interacting circular mesospins (square lattice, gap $g = 20$ nm) and varying diameter $D = [150, 250, 350, 450]$ nm, as a function of a vortex core displacement resulting from an applied field along the [10] lattice direction. The scaling of $E_v - E_c$ with the mesospin diameter, reveals a boundary between collinear (blue shade) and vortex (red shade) states as shown in the inset. The top of the figure illustrates how the core is moved with a distance of $2r$, leading to C states with varying degrees of magnetic texture until the collinear state is reached.

C. Directional dependence

Examples of the experimentally determined temperature dependence of the magnetization are displayed in Fig. 4 ($D = 350$ nm). The two different curves correspond to results obtained when applying the field in two different directions [10]

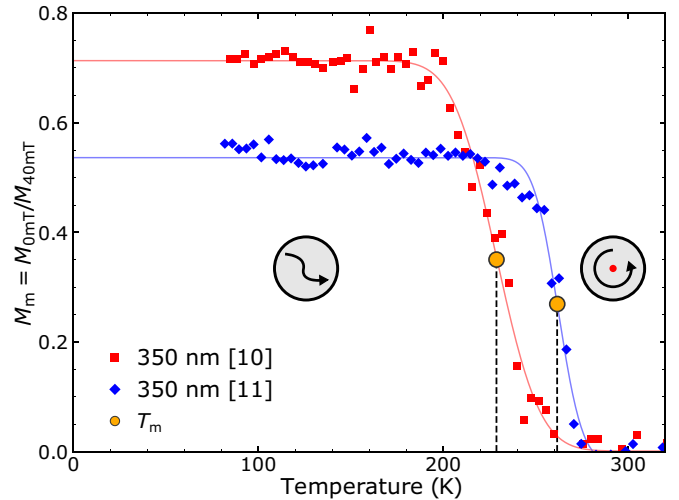


FIG. 4. Experimental results illustrating the directional dependence of $M_m = M_{0\text{mT}}/M_{40\text{mT}}$ as a function of temperature with external field applied along the [10] and [11] directions for mesospins with $D = 350$ nm. Error functions (solid lines) were chosen in order to determine the transition without assigning any physical interpretation to it. Yellow dots represent the transition temperature T_m separating the collinear like and vortex state, and illustrations exemplify possible internal states.

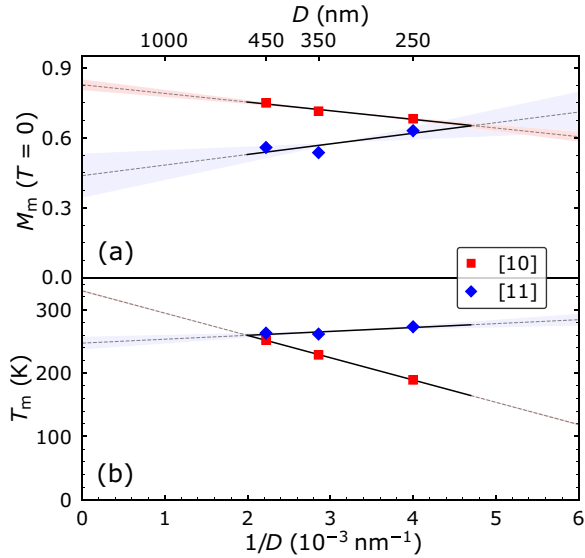


FIG. 5. Summary of the experimental findings: (a) the extent of magnetic texture, $M_m(T = 0)$, and (b) the transition temperature T_m separating the dressed and vortex state for $D = [250, 350, 450]$ nm along [10] and [11] direction. The error bars of the data are smaller than the symbols and are therefore not visible. The shaded areas represent the estimated uncertainty for the respective data sets.

and [11]. A plateau value of $M_m = 0.71(2)$ is obtained when the field has been applied along the [10] direction, whereas $M_m = 0.54(1)$ is obtained along the [11] direction. The lower magnetization of the array obtained when dressed along [11] is accompanied by a more stable configuration, manifested in a higher transition temperature. To allow for quantitative comparison, we define a transition temperature T_m defined as $M_m(T_m) = \frac{1}{2}M_m(T = 0)$. By this definition, $T_m = 229(1)$ K is obtained when the external field has been applied along [10] whereas $T_m = 261(1)$ K is obtained when the external field has been applied along the [11] direction.

Figure 5 shows the effect of the direction of the applied field on M_m and T_m for $D = [250, 350, 450]$ nm. The fits reveal linear relations with inverse mesospin diameter $1/D$. Positive slopes are observed when the external field has been applied along [11]. This is consistent with a decrease in magnetic texture (increasing M_T) with decreasing mesospin size and an increase in the transition temperature. When the field has been applied along the [10] direction, a decrease in M_m is obtained, accompanied by a profound decrease in T_m . Hence, the direction of the applied field results in a significant difference in the degree of magnetic texture and in the onset of the transition. The difference in response to an external field vanishes at diameters around 212 and 501 nm.

Figure 6 shows the normalized energy ($E/E_v - 1$) as a function of vortex core displacement for $D = [190, 250, 350, 450]$ nm dressed along the [10] (filled symbols) and the [11] directions (empty symbols). The ground state for mesospins with $D = 450$ nm is the vortex state, whereas the collinear state is metastable and independent of orientation. However, when inner magnetic textures, such as C states, are allowed, [10] and [11] are no longer equivalent, and the energy is observed to be lower when the net magnetization is along the [11] direction. Since the degree of

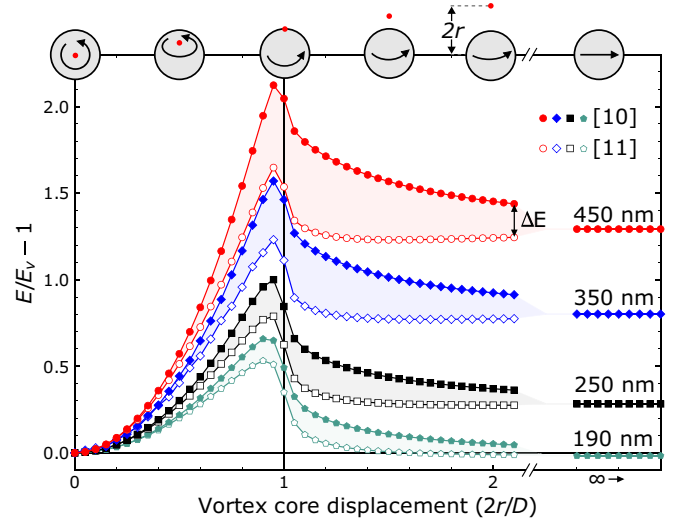


FIG. 6. The energy landscape of the transition between vortex and collinear states for mesospins arranged in a square lattice, having diameters of $D = [190, 250, 350, 450]$ nm and mesospin spacing of 20 nm. The energy has been normalized with respect to the vortex state with $E/E_v - 1 = 0$ when the vortex core is in the center of the disks. Numerical calculations were performed by moving the vortex core along a path [10] (filled symbols) or [11] (empty symbols) direction.





magnetic texture is equivalent for the two directions at any $2r/D$, the energy gap (ΔE) can only be associated with an energy gain mediated by magnetostatic coupling (E_j). This can be related to the experimental results observed in Fig. 5 where the transition temperature is higher when the external field has been applied along the [11] direction. Reducing the diameter to 250 and 350 nm does not have a remarkable effect on the energy landscape. Thus, a decrease in ΔE can be observed with size, and the energy associated with the interactions between the mesospins is less prominent. When the diameter is 190 nm, the energies for the vortex and collinear states are close to equivalent, and the directional dependence on magnetic texture is small.

D. The interplay of magnetic interactions and texture

The experimental results illustrated in Fig. 5 reveal changes in remanent magnetization and transition temperature with the size of the mesospins. To understand the causal relation, we need to take a closer look at how different magnetic textures affect the interactions of the mesospins. As illustrated in Table I, circularly shaped elements can accommodate internal magnetic textures, such as O, S, and C states as well as vortex states. The average magnetization ($|\langle \mathbf{m} \rangle|$) was determined for different configurations and sizes. There are noticeable differences between the net moment of the different states, whereas a weak trend is obtained in $|\langle \mathbf{m} \rangle|$ with size. We note a large scattering in the net moment when the elements are in S and C states. This scattering originates from the combination of large changes in the net moment of individual elements and the small sampling number in the simulations.

An example of an ensemble of magnetic elements and their stray field is illustrated in Fig. 7. The simulations correspond

TABLE I. Magnetic textures of V, O, S, and C states. The average magnetization $|\langle \mathbf{m} \rangle|$ is extracted along the horizontal axis of the illustrated states.

State	Diameter	$ \langle \mathbf{m} \rangle $
 V-state	250 nm	0
	350 nm	0
	450 nm	0
 O-state	250 nm	0.98
	350 nm	0.97
	450 nm	0.96
 S-state	250 nm	0.85(4)
	350 nm	0.92(3)
	450 nm	0.82(11)
 C-state	250 nm	0.64(3)
	350 nm	0.66(3)
	450 nm	0.61(4)

to a remnant state of 350-nm islands obtained after applying a field in the [10] and [11] directions. As seen in the figure, applying the field along the [10] direction gives rise to the exclusive presence of O states with large remnant magnetization and a clear but weak size dependence in the texture. The attractive interaction between the elements is exclusively along the [10] direction, thus, each element only interacts with its two nearest neighbors. Comparing $|\langle \mathbf{m} \rangle|$ for the O state in Table I and M_m in Fig. 5(a), reveals the presence of a smaller net moment in the experiments as compared to the simulations of the fully dressed mesospins. Furthermore, the simulations clearly show a decrease in remnant moment with decreasing element size, which is opposite to experimental observations. We, therefore, conclude that the decrease in the experimen-

tally determined remnant magnetization must originate from disorder arising from a rotation of the mesospins. The decrease in the transition temperature with decreasing size is in line with this conclusion because the rotation decreases the one-dimensional-like interaction.

When the field is applied in the [11] direction, the degree of order is lower, and both C and S states are observed as illustrated in Fig. 7(b). Furthermore, substantial rotation of the net moment of the elements is obtained. This effect contributes to the decrease in the remnant magnetization. Consequently, each element can interact with up to four of its nearest neighbors. The increase in the transverse magnetization, arising from the presence of C and S textures as well as rotation of the net moment, can, therefore, be concluded to be the cause of the smaller remnant magnetization obtained when applying the field in the [11] as compared to the [10] directions. At the same time, the interaction with up to four neighbors as compared to two can be viewed as the main cause for the stabilization of the metastable ferromagnetic state. Hence, a conceptual framework for the interplay of the interaction and magnetic texture within the mesospins is established.

IV. CONCLUSIONS

We provide experimental evidence of a configurational dependence in the energy of mesospins forming a square lattice, resulting in an emerging anisotropy in the interelement interactions. The effect of the anisotropy in the interaction energy [24,27–30] is determined from the directional dependence of the thermally induced transition from dressed ferromagnetic to vortex states. The key component required for rationalizing the results is an interplay between the interaction of the mesospins and their magnetic textures: When a mesospin and its neighbors have a net magnetization along [10] in the square lattice, the interaction can be viewed as being one dimensional along the same axis. When the net moment is along [11], the mesospins can effectively interact with up to four neighbors. These differences are caused by self-induced modifications of the inner magnetic texture, resulting in changes in mesospin interactions as illustrated by numeric simulations. The concepts presented in this paper, relating to the interplay of inter- and intramesospin length scales, can be viewed as a new way of designing emerging properties in magnetic metamaterials.

The data that support the findings are available from the corresponding authors upon reasonable request.

ACKNOWLEDGMENTS

We wish to thank Dr. S. D. Sløetjes for helpful discussions. B.H. and V.K. acknowledge financial support from the National Research Council (VR) (Projects No. 2019-03581 and No. 2019-05379). We acknowledge Myfab Uppsala for providing facilities and experimental support. Myfab is funded by the Swedish Research Council (Grant No. 2019-00207) as a national research infrastructure.

The authors have no conflicts to disclose.

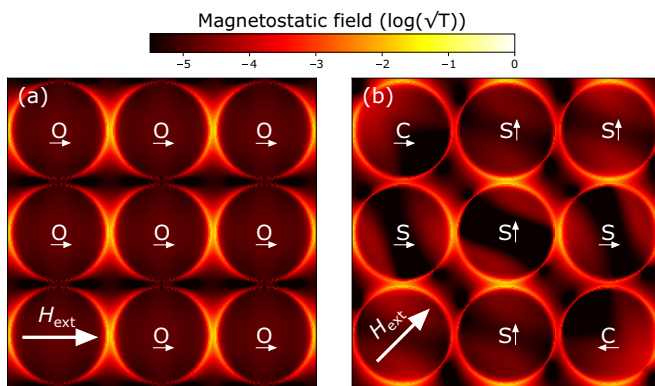


FIG. 7. Spatial maps of the stray field obtained from micromagnetic simulations of elements with diameters of 350 nm ($T = 0$). Initially the disks were saturated along [10] and [11] (H_{ext}) followed by relaxation in zero field (dressing). The lighter regions along the disk perimeters represent the strength of the interaction of the disks. The letters symbolize the magnetic texture (Table I), and arrows symbolize the orientation of $\langle \mathbf{m} \rangle$.

- [1] V. Kapaklis, U. B. Arnalds, A. Harman-Clarke, E. T. Papaioannou, M. Karimipour, P. Korelis, A. Taroni, P. C. W. Holdsworth, S. T. Bramwell, and B. Hjörvarsson, *New J. Phys.* **14**, 035009 (2012).
- [2] D. Levis, L. F. Cugliandolo, L. Foini, and M. Tarzia, *Phys. Rev. Lett.* **110**, 207206 (2013).
- [3] U. B. Arnalds, M. Ahlberg, M. S. Brewer, V. Kapaklis, E. T. Papaioannou, M. Karimipour, P. Korelis, A. Stein, S. Ólafsson, T. P. A. Hase, and B. Hjörvarsson, *Appl. Phys. Lett.* **105**, 042409 (2014).
- [4] U. B. Arnalds, J. Chico, H. Stopfel, V. Kapaklis, O. Bärenbold, M. A. Verschuuren, U. Wolff, V. Neu, A. Bergman, and B. Hjörvarsson, *New J. Phys.* **18**, 023008 (2016).
- [5] R. Streubel, N. Kent, S. Dhuey, A. Scholl, S. Kevan, and P. Fischer, *Nano Lett.* **18**, 7428 (2018).
- [6] N. Leo, S. Holenstein, D. Schildknecht, O. Sendetskyi, H. Luetkens, P. M. Derlet, V. Scagnoli, D. Lançon, J. L. Mardegan, T. Prokscha, A. Suter, Z. Salman, S. Lee, and L. J. Heyderman, *Nat. Commun.* **9**, 2850 (2018).
- [7] O. Sendetskyi, V. Scagnoli, N. Leo, L. Anghinolfi, A. Alberca, J. Lüning, U. Staub, P. M. Derlet, and L. J. Heyderman, *Phys. Rev. B* **99**, 214430 (2019).
- [8] S. H. Skjærvø, C. H. Marrows, R. L. Stamps, and L. J. Heyderman, *Nat. Rev. Phys.* **2**, 13 (2020).
- [9] B. E. Skovdal, N. Strandqvist, H. Stopfel, M. Pohlit, T. Warnatz, S. D. Sløetjes, V. Kapaklis, and B. Hjörvarsson, *Phys. Rev. B* **104**, 014434 (2021).
- [10] S. Gliga, A. Kákay, L. J. Heyderman, R. Hertel, and O. G. Heinonen, *Phys. Rev. B* **92**, 060413(R) (2015).
- [11] S. D. Sløetjes, B. Hjörvarsson, and V. Kapaklis, *Appl. Phys. Lett.* **118**, 142407 (2021).
- [12] S. D. Sløetjes, B. Hjörvarsson, and V. Kapaklis, *Phys. Rev. B* **106**, 104405 (2022).
- [13] H. Ding, A. Schmid, D. Li, K. Guslienko, and S. Bader, *Phys. Rev. Lett.* **94**, 157202 (2005).
- [14] E. Östman, U. B. Arnalds, E. Melander, V. Kapaklis, G. K. Pálsson, A. Y. Saw, M. A. Verschuuren, F. Kronast, E. T. Papaioannou, C. S. Fadley, and B. Hjörvarsson, *New J. Phys.* **16**, 053002 (2014).
- [15] T. Shinjo, T. Okuno, R. Hassdorf, K. Shigeto, and T. Ono, *Science* **289**, 930 (2000).
- [16] M. Kläui, C. A. F. Vaz, L. Lopez-Diaz, and J. A. C. Bland, *J. Phys.: Condens. Matter* **15**, R985 (2003).
- [17] J. K. Ha, R. Hertel, and J. Kirschner, *Phys. Rev. B* **67**, 224432 (2003).
- [18] J. K. Ha, R. Hertel, and J. Kirschner, *Phys. Rev. B* **67**, 064418 (2003).
- [19] B. E. Skovdal, G. K. Pálsson, P. C. W. Holdsworth, and B. Hjörvarsson, *arXiv:2204.10065*.
- [20] S. D. Sløetjes, H. H. Urdahl, J. K. Grepstad, and E. Folven, *AIP Adv.* **7**, 056325 (2017).
- [21] E. Digernes, S. D. Sløetjes, A. Strømberg, A. D. Bang, F. K. Olsen, E. Arenholz, R. V. Chopdekar, J. K. Grepstad, and E. Folven, *Phys. Rev. Res.* **2**, 013222 (2020).
- [22] E. Digernes, A. Strømberg, C. A. F. Vaz, A. Kleibert, J. K. Grepstad, and E. Folven, *Appl. Phys. Lett.* **118**, 202404 (2021).
- [23] A. Vansteenkiste and B. Van de Wiele, *J. Magn. Magn. Mater.* **323**, 2585 (2011).
- [24] A. Ciuculkaite, E. Östman, R. Brucas, A. Kumar, M. A. Verschuuren, P. Svedlindh, B. Hjörvarsson, and V. Kapaklis, *Phys. Rev. B* **99**, 184415 (2019).
- [25] A. Vansteenkiste, J. Leliaert, M. Dvornik, M. Helsen, F. Garcia-Sanchez, and B. Van Waeyenberge, *AIP Adv.* **4**, 107133 (2014).
- [26] R. P. Cowburn, D. K. Koltsov, A. O. Adeyeye, M. E. Welland, and D. M. Tricker, *Phys. Rev. Lett.* **83**, 1042 (1999).
- [27] C. Mathieu, C. Hartmann, M. Bauer, O. Buettner, S. Riedling, B. Roos, S. O. Demokritov, B. Hillebrands, B. Bartenlian, C. Chappert, D. Decanini, F. Rousseaux, E. Cambril, A. Müller, B. Hoffmann, and U. Hartmann, *Appl. Phys. Lett.* **70**, 2912 (1997).
- [28] M. Natali, A. Lebib, Y. Chen, I. L. Prejbeanu, and K. Ounadjela, *J. Appl. Phys.* **91**, 7041 (2002).
- [29] G. N. Kakazei, Y. G. Pogorelov, M. D. Costa, T. Mewes, P. E. Wigen, P. C. Hammel, V. O. Golub, T. Okuno, and V. Novosad, *Phys. Rev. B* **74**, 060406(R) (2006).
- [30] X. Zhu, P. Grütter, V. Metlushko, and B. Ilic, *Appl. Phys. Lett.* **80**, 4789 (2002).